Hindawi Publishing Corporation
EURASIP Journal on Image and Video Processing
Volume 2010, Article ID 874364, 14 pages
doi:10.1155/2010/874364

Research Article

Edge Adaptive Color Demosaicking Based on the Spatial Correlation of the Bayer Color Difference

Hyun Mook Oh, Chang Won Kim, Young Seok Han, and Moon Gi Kang

TMS Institute of Information Technology, Yonsei University, 134 Shinchon-Dong, Seodaemun-Gu, Seoul 120-749, Republic of Korea

Correspondence should be addressed to Moon Gi Kang, mkang@yonsei.ac.kr

Received 10 April 2010; Revised 25 June 2010; Accepted 24 September 2010

Academic Editor: Lei Zhang

An edge adaptive color demosaicking algorithm that classifies the region types and estimates the edge direction on the Bayer color filter array (CFA) samples is proposed. In the proposed method, the optimal edge direction is estimated based on the spatial correlation on the Bayer color difference plane, which adopts the local directional correlation of an edge region of the Bayer CFA samples. To improve the image quality with the consistent edge direction, we classify the region of an image into three different types, such as edge, edge pattern, and flat regions. Based on the region types, the proposed method estimates the edge direction adaptive to the regions. As a result, the proposed method reconstructs clear edges with reduced visual distortions in the edge and the edge pattern regions. Experimental results show that the proposed method outperforms conventional edge-directed methods on objective and subjective criteria.

1. Introduction

Single chip CCD or CMOS imaging sensors are widely used in digital still cameras (DSCs) to reduce the cost and size of the equipments. Such imaging sensors obtain pixel information through a color filter array (CFA), such as Bayer CFA [1]. When the Bayer CFA is used in front of the image sensor, one of the three spectral components (red, green, or blue) is passed at each pixel location as shown in Figure 1(a). In order to obtain the full color image, the missing color components should be estimated from the existing pixel information. This reconstruction process is called *color demosaicking* or *color interpolation* [2–25]. Generally, the correlation between color channels is utilized by assuming the smoothness color ratio [3, 4] or smoothness color difference [5–7]. These methods produce satisfactory results in a homogeneous region, while visible artifacts (such as zippers, Moiré effects, and blurring artifacts) are shown in edge regions.

In order to reduce interpolation errors in these regions, various approaches have been applied to color demosaicking. In [8–12], various edge indicators were used to prevent interpolation across edges. Gunturk et al. decomposed color channels into frequency subbands and updated the high-frequency subbands by applying a projection onto convex-sets (POCS) technique [13]. Zhang and Wu modeled color artifacts as noise factors and removed them by fusing the directional linear minimum mean squares error (LMMSE) estimates [14]. Alleysson et al. proposed frequency selective filters which adopt localization of the luminance and chrominance frequency components of a mosaicked image [15]. All of these approaches show highly improved results on the edge regions. However, the interpolation error and smooth edges in edge patterns or edge junctions are challenging issues in demosaicking methods.

As an approach to reconstruct the sharp edge, edge directed color demosaicking algorithms were proposed which aimed to find the optimal edge direction at each pixel location [16–25]. Since the interpolation is performed along the estimated edge direction, the edge direction estimation techniques play a main roll in these methods. In some methods [20–22], the edge directions of missing pixels are indirectly estimated in aid of the additional information from the horizontally and vertically prereconstructed images. Wu and

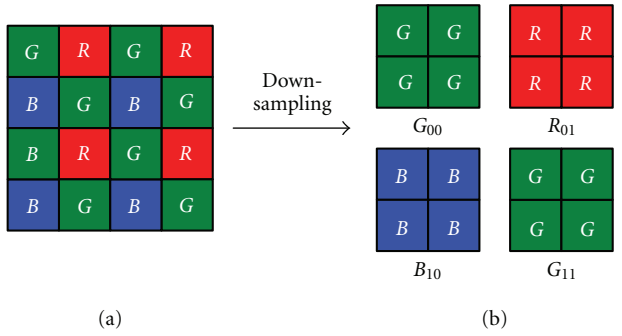

Figure 1: (a) The Bayer CFA pattern and (b) the down sampled low resolution images.

Zhang found the edge direction based on the Fisher's linear discriminant so that the chance of the misclassification of each pixel is minimized [20]. Hirakawa and Parks proposed a homogeneity map-based estimation process, which adopted the luminance and chrominance similarities between the pixels on an edge [21]. Menon et al. proposed the direction estimation scheme using the smoothness color differences on the edges, where the color difference was obtained based on the directionally filtered green images [22]. In these methods, the sharp edges are effectively restored with the temporally interpolated images. However, the insufficient consideration for the competitive regions results in outstanding artifacts due to the inconsistent directional edge interpolation.

Recently, some methods that directly deal with the CFA problems such as CFA sampling [23–25], CFA noise [26] or both of the problems [27] were proposed. These methods studied the characteristics of the CFA samples and reconstructed the image without the CFA error propagation and the inefficient computations due to the preinterpolation process. Focusing on the demosaicking directly on the CFA samples, Chung and Chan studied the color difference variance of the pixels located along the horizontal or the vertical axis of CFA samples [23]. Tsai and Song introduced the concept of the spectral-spatial correlation (SSC) which represented the direct difference between Bayer CFA color samples [24]. Based on the SSC, they proposed heterogeneity-projection technique that used the smoothness derivatives of the Bayer sample differences on the horizontal or vertical edges. Based on the Tsai and Song's method, Chung et al. proposed modified heterogeneity-projection method that adaptively changed the mask size of the derivative [25].

As shown in [24, 25], difference of the Bayer samples provides key to directly estimate the edge direction on the Bayer pattern. In the conventional SSC-based methods, the smoothness of the Bayer color difference along an edge is examined, and the derivative of the differences along the horizontal or vertical axis is adopted as a criterion for edge direction estimation. However, in the complicated edge region, such as edge patterns or edge junctions, the edge direction is usually indistinguishable since derivatives along the line are very close to the horizontal and vertical directions. To carry out more accurate interpolation on these regions, region adaptive interpolation scheme which estimates the edge direction adaptive to the region types with the given directional correlation on Bayer color difference is required.

In this paper, a demosaicking method that estimates the edge direction directly on the Bayer CFA samples is proposed based on the spatial correlation of the Bayer color difference. To estimate the edge direction with accuracy, we investigate the consistency of the Bayer color difference within a local region. We focus on the local similarity of the Bayer color difference plane not only along the directional axis but also beside the axis within the local region. Since the edge directions of the pixels on and around the edge contribute to the estimation simultaneously, the correlation adopted in the proposed method is a stable and effective basis to estimate the edge direction in the complicated edge regions. Based on the spatial correlation on the Bayer color difference plane, we propose an edge adaptive demosaicking method that classifies an image into edge, edge pattern, and flat regions, and that estimates the edge direction according to the region type. From the result of the estimated edge direction, the proposed method interpolates the missing pixel values along the edge direction.

The rest of the paper is organized as follows. Using the difference plane of the down sampled CFA images, the spatial correlation on the Bayer color difference plane is examined in Section 2. Based on the examined correlation between the CFA sample differences, the proposed edge adaptive demosaicking method is described with the criteria for the edge direction detection and the region classification in Section 3. Also, the interpolation scheme along the estimated edge direction is depicted, which aims to restore the missing pixels with reduced artifacts. Section 4 presents comparisons between the proposed and conventional edge directed methods in terms of the quantitative and qualitative criteria. Finally, the paper is concluded with Section 5.

2. Spatial Correlation on the Bayer Color Difference Plane

In the proposed method, the region type and the edge direction are determined directly on the Bayer CFA samples based on the correlation of the Bayer color difference. For the efficient criteria for these main parts of the proposed demosaicking method, the Bayer color difference is reexamined on the down sampled low-resolution (LR) Bayer image plane so that the direction-oriented consistency of the Bayer color differences is emphasized within the local region of an edge.

The Bayer color difference is a strong relation between the CFA samples on a horizontal or vertical line [24], followed as

$$\begin{aligned} D_{rg}^{h(j,j+1)} &= R(i,j) - G(i,j+1) \\ &= \left(R(i,j) - \hat{G}(i,j)\right) - \left(G(i,j+1) - \hat{G}(i,j)\right), \\ D_{rg}^{v(i,i+1)} &= R(i,j) - G(i+1,j) \\ &= \left(R(i,j) - \hat{G}(i,j)\right) - \left(G(i+1,j) - \hat{G}(i,j)\right), \end{aligned} \tag{1}$$

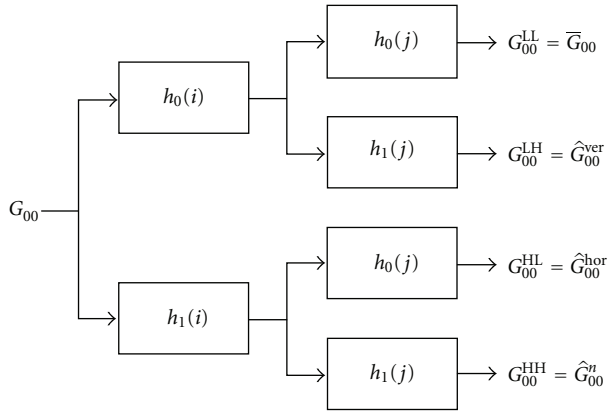

Figure 2: Undecimated 2D wavelet transform with filter banks and spectral components of G_{00}.

where the $R(i, j)$, and $G(i, j)$ are Bayer CFA samples of red and green channels in (i, j) pixel location, respectively, $\hat{G}(i, j)$ is a missing sample of green channel, and $D_{rg}^{h(j,j+1)}$ and $D_{rg}^{v(i,i+1)}$ are the Bayer color difference on the horizontal and vertical directional lines, respectively. The Bayer color difference is assumed piecewise constant along an edge since it inherits the characteristics of spectral and spatial correlations [24].

From the relation between the CFA samples on a line, we expand the CFA sample relation into the Bayer color difference plane which is defined by the difference of Bayer LR images. When we consider the down sampling of the Bayer CFA image as shown in Figure 1, each of the LR image is obtained according to the sampling position of each color channel, given as

$$C_{xy}(i, j) = \mathrm{CFA}(2i + x, 2j + y), \tag{2}$$

where $\mathrm{CFA}(i, j)$ represent the Bayer CFA samples at pixel index (i, j) and the LR image channel C is green, red, blue, and green channels according to the sampling index $\{(x, y) \mid (0, 0), (0, 1), (1, 0), (1, 1)\}$, respectively. Therefore, we obtain four LR images $\{G_{00}, R_{01}, B_{10}, G_{11}\}$, and each of them has full spatial resolution in LR grid as shown in Figure 1(b). Using the defined LR images, the Bayer color difference plane is defined as the difference between the LR images,

$$D_{C1_{xy}C2_{zw}} = C1_{xy} - C2_{zw}, \tag{3}$$

where $D_{C1_{xy}C2_{zw}}$ is the Bayer color difference plane given the different Bayer LR images, $C1_{xy} \neq C2_{zw}$. Note that, the correlation between the sampling positions are simultaneously considered with the inter channel correlation in (3).

To describe the local property of $D_{C1_{xy}C2_{zw}}$, we consider the directional components of LR images. When we use the undecimated wavelet transform, a LR image can be decomposed into low-frequency, horizontal, vertical directional and the residual high frequency components [13]. As shown in Figure 2, the two-staged directional low-pass and the high-pass filters, $h_0(i)$ and $h_1(j)$, respectively, make the low-pass and directionally high-pass filtered images. Given the directional forward filter banks, a Bayer LR image C_{xy} is represented as the sum of four frequency components, such as,

$$\begin{aligned} C_{xy} &= C_{xy}^{\mathrm{LL}} + C_{xy}^{\mathrm{LH}} + C_{xy}^{\mathrm{HL}} + C_{xy}^{\mathrm{HH}} \\ &\approx \overline{C}_{xy} + \hat{C}_{xy}^{\mathrm{ver}} + \hat{C}_{xy}^{\mathrm{hor}}, \end{aligned} \tag{4}$$

where the upper letters LL, LH, HL, HH represent the low frequency, vertical and horizontal directional high frequencies, and the residual components of C_{xy}, respectively, and they are described as $\overline{C}_{xy}$, $\hat{C}_{xy}^{\mathrm{ver}}$, and $\hat{C}_{xy}^{\mathrm{hor}}$. In (4), it is assumed that the most of the high-frequencies of an image is concentrated on the vertical and horizontal directional components, so that the residual parts are not considered in the following discussion. Also, the directional high frequency components are assumed to be exclusively separated in the horizontal and vertical directions, since an image has strong directional correlation along the sharp edges. Therefore, $\hat{C}_{xy}^{\mathrm{hor}}$ (or $\hat{C}_{xy}^{\mathrm{ver}}$) is approximately zero in the vertical (or horizontal) sharp edge region in (4). Based on these assumptions, the Bayer color difference plane in (3) is reorganized as follows,

$$\begin{aligned} D_{C1_{xy}C2_{zw}} &= C1_{xy} - C2_{zw} \\ &\approx K + (1 - \delta(x - z))\left(\widehat{C1}_{xy}^{\mathrm{hor}} - \widehat{C1}_{zw}^{\mathrm{hor}}\right) \\ &\quad + (1 - \delta(y - w))\left(\widehat{C1}_{xy}^{\mathrm{ver}} - \widehat{C1}_{zw}^{\mathrm{ver}}\right), \end{aligned} \tag{5}$$

where $K = C1_{zw} - C2_{zw}$ represents the spectral correlation between the Bayer LR images [7], and $\delta(a - b)$ indicates the LR image shift direction where the value 1 for $a = b$ represents no shift, and 0 for $a \neq b$ represents the shift toward the direction. Note that, the horizontal (or vertical) directional frequency components are paired with the vertical (or horizontal) directional shifting indicator. The cross-directional pair of shift indicator and the directional frequencies shows the relation between the global LR image shifting direction and the local edge direction: the Bayer color difference is highly correlated in a local region when the global shift and the local edge directions are corresponded to each other. We call it as the spatial correlation of the Bayer color difference.

In Figure 3, a vertical edge region is shown as an example of the relation between the global and the local directions. When the vertical region in the 6×6 local region of Bayer pattern in Figure 3(a) is down sampled, the corresponding LR images in Figure 3(b) show different edge locations according to the sampling location. When the global shift direction coincides with the vertical local direction, Bayer LR images show similar edge location. Otherwise, the edges in each image are dislocated. From (5), the Bayer color difference planes that is obtained by R_{01} and horizontally and vertically shifted images G_{00} and G_{11}, respectively, are given as follows:

$$\begin{aligned} D_{G_{00}R_{01}} &= K + \widehat{C1}_{xy}^{\mathrm{ver}} - \widehat{C1}_{zw}^{\mathrm{ver}} \\ D_{G_{11}R_{01}} &= K. \end{aligned} \tag{6}$$

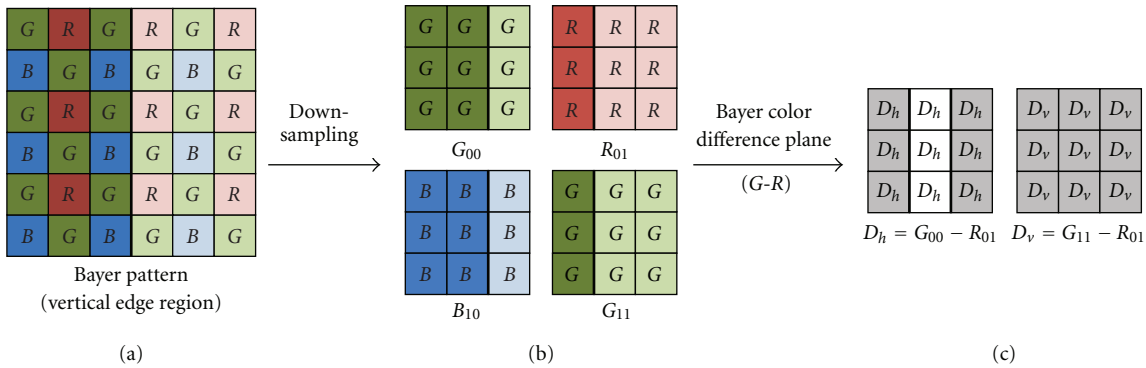

Figure 3: Vertical edge region of (a) Bayer CFA samples, (b) Bayer LR images, and (c) the Bayer color difference planes.

In (6), the difference of vertical high frequency components are remained in the difference of horizontally shifted LR images, while they are disappeared in the difference of vertically shifted LR images. In the real images, the spatial correlation on the Bayer color difference plane can be shown as depicted in Figure 4. In the strong vertical edge region in Figure 4(a), the difference plane obtained from the vertically shifted LR images is smooth planes, while the difference obtained from the horizontally shifted images shows overstated details. In the edge pattern region in Figure 4(b), the aliasing effect of the LR images makes pattern in the difference plane from the horizontally shifted images. However, the aliasing effects are disappeared in the difference plane of the opposite case. From these examples, the strong connection of the global shift direction and the local edge direction is described by the spatial correlation of Bayer color difference. In the following section, we describe the detailed method to use the spatial correlation of the Bayer color difference in the edge direction estimation and the region classification.

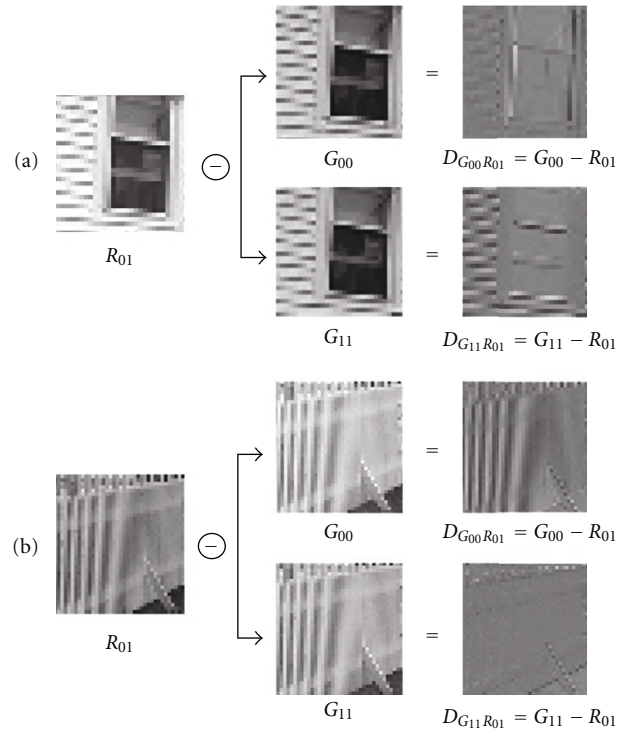

Figure 4: Examples of the Bayer color difference planes of R_{01} and G_{00} and R_{01} and G_{11} (a) edge and flat regions (b) vertical edge pattern region.

3. Proposed Edge Directed Color Demosaicking Algorithm Using Region Classifier

In the proposed edge adaptive demosaicking method, the edge directions are optimally estimated according to the region type. Based on the spatial correlation of the Bayer color difference, the proposed method classifies an image into three regions, such as edge, edge pattern, and flat regions. In each of the regions, we classify the edge direction type (EDT) as the horizontal (Hor) or vertical (Ver) direction. When the direction is not obviously determined, we decide the direction as nondirectional (Non). Therefore, the final types of the edge direction are EDT = {Hor, Ver, Non}. In the proposed edge direction estimation, the diagonal directional edge is considered as the combination of the horizontal and vertical directional edges. According to the determined edge direction, the missing pixels are interpolated with weighting functions. Following the edge types and the edge directions, we present the way to classify the region and to estimate the edge direction based on the spatial correlation on the Bayer color difference plane. To utilize the correlation, we describe the details of the interpolation process as the restoration of missing channels of LR images. Given the obtained LR images BAYER = $\{G_{00}, R_{01}, B_{10}, G_{11}\}$ in Figure 1(b), the missing channels of each LR color images are $\{G_{01}, G_{10}, R_{00}, R_{10}, R_{11}, B_{00}, B_{01}, B_{11}\}$. By considering the sampling rate of the green channel, the proposed method first interpolates the missing green channels, than the red and blue channels are interpolated by using the fully interpolated green channel images. This is helpful to improve the red and blue channel interpolation quality, since the green channel has more edge information than the red and blue channels. Since the Bayer LR images are shifted to each other, they are interpolated in the same way for each channel.

Once all of the missing channels are reconstructed at each sampling position, the full-color LR images are upsampled and they are registered according to the original position in the HR grid. The overall process of the proposed adaptive demosaicking method is depicted in Figure 6, where the process is composed of estimating Bayer color difference plane, the region classification, the edge direction estimation, and the directional interpolation for each green and red/blue channel interpolation. In the following subsections, the way of interpolating the missing pixels in G_{01} and R_{00} are described as a representative of green and red(blue) channel interpolations.

3.1. Green Channel Interpolation

3.1.1. Region Classification: Sharp Edges. In the proposed demosaicking method, the modified notation for the sampling index is used to emphasize the relation between the global shift direction and local edge direction in LR images. When we consider the interpolation of the missing green channel of R_{01} position, we set the red pixel position as the center position, that is,

$$R_c(i,j) = \mathrm{CFA}(2i, 2j+1) = R_{01}(i,j). \tag{7}$$

According to the center position, the four neighborhood positions are defined as

$$\begin{aligned} G_{\mathrm{n}}(i,j) &= \mathrm{CFA}(2i-1, 2j+1) = G_{11}(i-1,j), \\ G_{\mathrm{s}}(i,j) &= \mathrm{CFA}(2i+1, 2j+1) = G_{11}(i,j), \\ G_{\mathrm{e}}(i,j) &= \mathrm{CFA}(2i, 2j+2) = G_{00}(i,j+1), \\ G_{\mathrm{w}}(i,j) &= \mathrm{CFA}(2i, 2j) = G_{00}(i,j), \end{aligned} \tag{8}$$

where $\{n, s, e, w\}$ represents the position of the pixels in the LR images in the north, south, east, and west from the center position. Note that the notation inherits the relative pixel position in Bayer CFA samples from the center pixel position.

Using the modified notation, the Bayer color difference in (3) is defined as

$$D_{G_pR_{\mathrm{c}}}(i,j) = G_p(i,j) - R_{\mathrm{c}}(i,j), \tag{9}$$

where $p = \{n, s, e, w\}$. From the spatial correlation on the Bayer color difference plane in (5), $D_{G_pR_{\mathrm{c}}}$ is highly correlated in the local region when the shifting direction coincides with the local edge direction. As an estimator for the spatial correlation, the local variations of the difference is estimated, such as

$$v_{\mathrm{p}}(i,j) = \sum_{(k,l)\in N} \left| D_{G_pR_{\mathrm{c}}}(i+k, j+l) - D_{G_pR_{\mathrm{c}}}(i,j) \right|, \tag{10}$$

where $N = \{(k,l) \mid -1 \le k,l \le 1, (k,l) \ne (0,0)\}$. In Figure 5, the window mask on the Bayer pattern and the corresponding Bayer color difference planes are described. When the local variations of each position are determined,

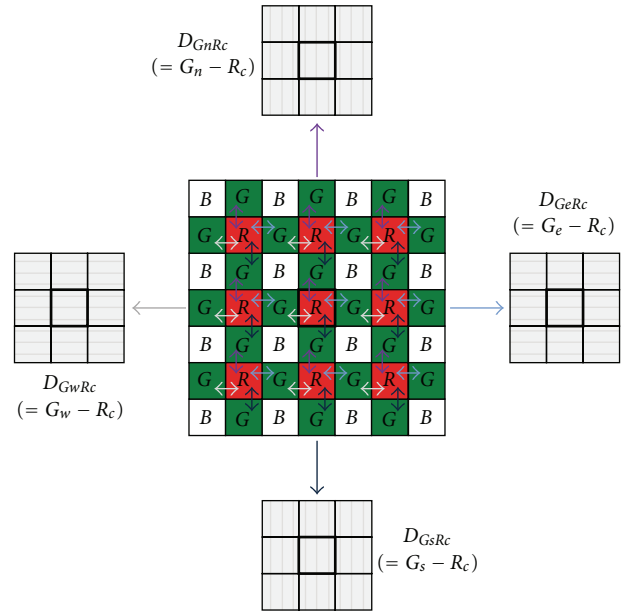

Figure 5: A 7×7 window of Bayer CFA pattern and its four neighboring Bayer color difference planes for local variation criterion.

the maximum and the minimum variations of horizontal shifting direction are defined as:

$$\begin{aligned} v_{\mathrm{hor}}^{\max}(i,j) &= \mathbf{MAX}[v_{\mathrm{w}}(i,j), v_{\mathrm{e}}(i,j)], \\ v_{\mathrm{hor}}^{\min}(i,j) &= \mathbf{MIN}[v_{\mathrm{w}}(i,j), v_{\mathrm{e}}(i,j)]. \end{aligned} \tag{11}$$

Also, $v_{\mathrm{ver}}^{\max}(i,j)$ and $v_{\mathrm{ver}}^{\min}(i,j)$ are determined as the same way in (11) by changing $\{v_{\mathrm{w}}, v_{\mathrm{e}}\}$ to $\{v_{\mathrm{s}}, v_{\mathrm{n}}\}$. The edge direction is clearly determined owing to the group with smaller variations, since the maximum of local variations along the edge direction is smaller than the minimum of local variations across the edge direction in the strong edge region.

In addition, the spatial similarity between the green channels is estimated for the restrict decision of the edge direction. Defining the difference plane of green channel,

$$D_{G_pG_q}(i,j) = G_p(i,j) - G_q(i,j), \tag{12}$$

where $\{(p,q) \mid (e,w), (n,s)\}$ is a pair of the horizontally or vertically located LR image positions. By applying the discussions in (5), the spatial correlation of $D_{G_pG_q}$ is estimated by the local similarity for the horizontal and the vertical directions, such as,

$$\begin{aligned} \rho_{\mathrm{hor}}(i,j) &= \sum_{k=-1}^{1} \sum_{l=-1}^{1} \left| D_{G_{\mathrm{w}}G_{\mathrm{e}}}(i+k, j+l) \right|, \\ \rho_{\mathrm{ver}}(i,j) &= \sum_{k=-1}^{1} \sum_{l=-1}^{1} \left| D_{G_{\mathrm{n}}G_{\mathrm{s}}}(i+k, j+l) \right|, \end{aligned} \tag{13}$$

where $\rho_{\mathrm{hor}}(i,j)$ and $\rho_{\mathrm{ver}}(i,j)$ represent the local average of the differences between the horizontally and vertically shifted green images, respectively. The local similarity becomes small

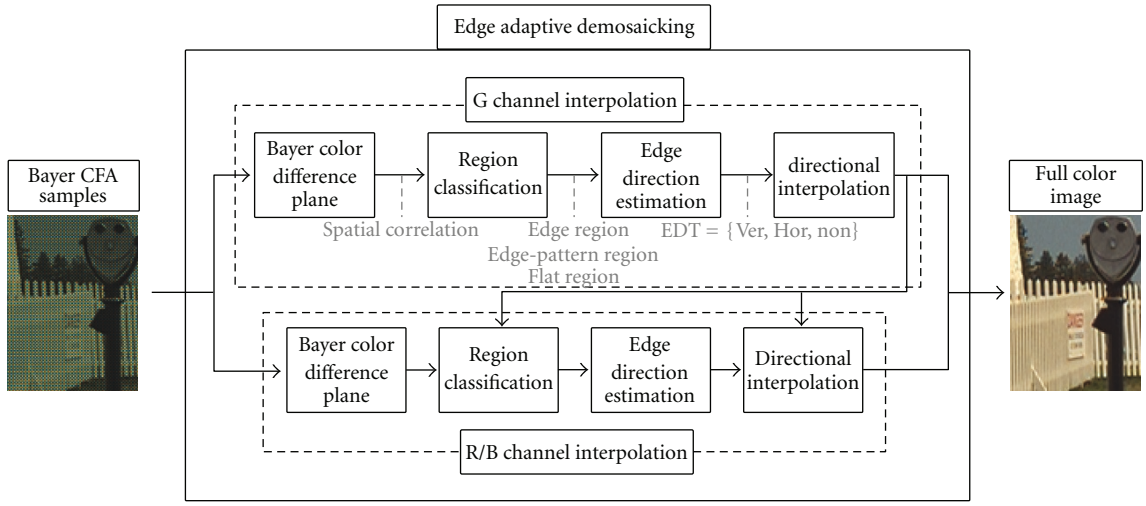

Figure 6: Flowchart of the proposed edge adaptive color demosaicking algorithm.

when the global shift and the local edge directions are coincided.

With the measured local variation and local similarity criteria, the EDT of each pixel is determined by,

Classification 1. Sharp edge region

$$\text{EDT} = \begin{cases} \text{Hor} & \\ \quad \text{if } v_{\text{hor}}^{\max} < v_{\text{ver}}^{\min} \text{ and } \rho_{\text{hor}} < \rho_{\text{ver}}, & \\ \text{Ver} & \\ \quad \text{if } v_{\text{hor}}^{\min} > v_{\text{ver}}^{\max} \text{ and } \rho_{\text{hor}} > \rho_{\text{ver}}, & \\ (\text{nonsharp edge region}), & \\ \quad \text{otherwise}, & \end{cases} \tag{14}$$

where Hor and Ver represents the sharp edges along horizontal or vertical directions, respectively. When the direction is not determined, the region is considered as a nonsharp edge region and these regions are investigated again in the following region classification step: *Classification 2*.

3.1.2. Region Classification: Edge Patterns. The regions of which edge types are not determined in (14) belong to the flat or the edge pattern region. The edge pattern region represents the region in the HR image that contains high-frequency components above the Nyquist rate of the Bayer CFA sampling. When the image is down sampled, the high frequency components that exceed the sampling rate are contaminated due to the aliasing effect. Therefore, the edge pattern region appears as locally flat in the LR image as shown in Figure 4(b). In this section, we derive the detection rule for the edge pattern region (pseudoflat region in the LR grid) and estimate the edge direction of the edge pattern.

To distinguish the pseudoflat region from the flat region, we use the characteristics of aliasing effect in the LR images. As shown in Figure 4(b), the fence region of G_{00} and G_{11} are flat for each images. This phenomenon is caused by the CFA sampling above the Nyquist rate in these regions and the high frequencies in HR image is blended into the low frequency by the down sampling. However, they are not the same flat when we compare the intensity of them at the same pixel location since the frequency blending cannot contaminate the intensity offset between the adjacent edges. Therefore, we use two criteria to classify the pseudoflat region from the normal flat region: the intensity offset and the smoothness restriction. The intensity offset is estimated by

$$\mu(i,j) = \left| \frac{\overline{G}_{\text{n}}(i,j) + \overline{G}_{\text{s}}(i,j)}{2} - \frac{\overline{G}_{\text{e}}(i,j) + \overline{G}_{\text{w}}(i,j)}{2} \right|, \tag{15}$$

where $\mu(i,j)$ is the difference between averages of the horizontally and vertically located LR images, and $\overline{G}_p(i,j)$ represents the low frequency of G_p at (i,j) pixel location. In addition to intensity offset, we restrict the condition with the pixel smoothness in respective LR images. Since we deal with the flat (and also the pseudoflat) region, the local variation values, which mean the fluctuation on each of the difference images, should be similar to each other. The similarity between the local variation values is estimated by the standard deviation of the local variations, given by:

$$\sigma_v(i,j) = \sqrt{\frac{1}{4}\sum_p \left(v_p(i,j) - \overline{v}(i,j)\right)^2}, \tag{16}$$

where $\sigma_v(i,j)$ is a variation of $v_p(i,j)$ and $\overline{v}(i,j)$ is the average of local variations.

With the intensity offset and the restrictive condition, the pseudoflat region (edge pattern region) is classified from the nonsharp edge region, such as

Classification 2. Edge pattern or Flat region

$$\mathrm{EDT} = \begin{cases} (\text{edge pattern}) & \text{if } \mu > th1,\ \sigma_v < th2, \\ \text{Non} & \text{otherwise}, \end{cases} \tag{17}$$

where edge pattern and Non represent that the region is determined as the edge pattern region and a flat region in this classification, respectively, and $th1$ and $th2$ are thresholds that control the accuracy of the classification. If μ is larger (and σ_v is smaller) than the threshold, the pixel at (i, j) is considered as being in the edge pattern region and the direction of the edge pattern is determined by the following criteria.

For pixels classified into the edge pattern region, the pattern edge direction is estimated using the modified local variation values in (10) with the extended range $N = \{(k, l) \mid -2 \le k, l \le 2, (k, l) \ne (0, 0)\}$. The edge direction of the edge pattern region is estimated as

$$\mathrm{EDT} = \begin{cases} \text{Hor} & \text{if } v_{\text{hor}}^{\max} < v_{\text{ver}}^{\min} \\ \text{Ver} & \text{if } v_{\text{hor}}^{\min} > v_{\text{ver}}^{\max} \\ \text{Non} & \text{otherwise}, \end{cases} \tag{18}$$

where Hor and Ver represent that the edge pattern is horizontally or vertically directed, respectively, and Non represents the region of which the edge direction is not clearly determined. Once the edge type of the edge pattern region is determined, the statistics of neighboring edge directions, such as the horizontal or vertical direction, are compared within a neighborhood. Following the majority of the directions, the consistency of the edge directions in the region is improved.

3.1.3. Edge Directed Interpolation. After the edge types of all pixels are categorized with the classified region types, edge directed interpolation is performed. If the edge types are clearly determined as Hor or Ver, the missing pixels are interpolated toward the direction. When the edge direction is determined as Non, it is considered as the flat region or the region where the edge direction is not defined. In this case, the missing pixels are interpolated by the weighted average of neighboring pixels. Therefore, the missing green channel LR image is interpolated according to the edge types, such as,

$$G_{01} = \begin{cases} \dfrac{\omega_{\mathrm{e}} K_{\mathrm{e}}^{\mathrm{R}} + \omega_{\mathrm{w}} K_{\mathrm{w}}^{\mathrm{R}}}{\omega_{\mathrm{e}} + \omega_{\mathrm{w}}} + R_c & \text{if EDT} = \text{Hor}, \\ \dfrac{\omega_{\mathrm{n}} K_{\mathrm{n}}^{\mathrm{R}} + \omega_{\mathrm{s}} K_{\mathrm{s}}^{\mathrm{R}}}{\omega_{\mathrm{n}} + \omega_{\mathrm{s}}} + R_c & \text{if EDT} = \text{Ver}, \\ \dfrac{(\omega_{\mathrm{n}} K_{\mathrm{n}}^{\mathrm{R}} + \omega_{\mathrm{s}} K_{\mathrm{s}}^{\mathrm{R}} + \omega_{\mathrm{e}} K_{\mathrm{e}}^{\mathrm{R}} + \omega_{\mathrm{w}} K_{\mathrm{w}}^{\mathrm{R}})}{(\omega_{\mathrm{n}} + \omega_{\mathrm{s}} + \omega_{\mathrm{e}} + \omega_{\mathrm{w}})} + R_c & \text{if EDT} = \text{Non}, \end{cases} \tag{19}$$

where ω_p represent a weight function, and K_p^{R} is a color difference domain value obtained from four green LR image locations. The weighting function used in the interpolation process is a reciprocal of gradient magnitude values [10]:

$$\omega_p(i, j) = \frac{1}{1 + \Delta_{\mathrm{c}} + \Delta_{\mathrm{d1}} + \Delta_{\mathrm{d2}}}, \tag{20}$$

where Δ_{c}, Δ_{d1} and Δ_{d2} represent the gradients of the pixels in the center image, in the LR images that are shifted corresponding to the considering direction p, and in the other LR images, respectively. For example, the weighting function in the north direction $\omega_{\mathrm{n}}(i, j)$ is calculated from $\Delta_{\mathrm{c}} = |R_{\mathrm{c}}(i-1, j) - R_{\mathrm{c}}(i, j)|$, $\Delta_{\mathrm{d1}} = |G_{\mathrm{n}}(i-1, j) - G_{\mathrm{n}}(i, j)| + |G_{\mathrm{s}}(i-1, j) - G_{\mathrm{s}}(i, j)|$, and $\Delta_{\mathrm{d2}} = |G_{\mathrm{e}}(i-1, j) - G_{\mathrm{e}}(i, j)| + |G_{\mathrm{w}}(i-1, j) - G_{\mathrm{w}}(i, j)|$. The K_p^{R} values of each LR image are obtained as followed by using the definition of the difference between the red and green channels [7]:

$$K_p^{\mathrm{R}}(i, j) = \frac{G_p(i, j) - R_{\mathrm{c}}(i, j) + R_{\mathrm{c}}(i + a, j + b)}{2}, \tag{21}$$

where $\{(a, b) \mid (-1, 0), (1, 0), (0, -1), (0, 1)\}$ is for $\{p \mid \mathrm{n}, \mathrm{s}, \mathrm{e}, \mathrm{w}\}$, respectively.

3.2. Red and Blue Channel Interpolation. Similar to the green plane interpolation, the missing red and blue channel LR images are interpolated along the edge direction by the region classification and the edge direction estimation. The fully interpolated green channels which have much information on edges are utilized to improve interpolation accuracy of the red and blue channels. To compensate insufficient LR images, the diagonally shifted LR images of $\{R_{01}, B_{10}\}$ are estimated using linear interpolation on the color difference domain [7]. In this section, the missing red and blue channels $\{R_{00}, R_{11}, B_{00}, B_{11}\}$ are found in aid of the sampled images $\{G_{00}, G_{11}, R_{01}, B_{10}\}$ and the interpolated images $\{G_{01}, G_{10}, R_{10}, B_{01}\}$.

To interpolate the red LR image in $(0, 0)$ sampling position, G_{00} is used as the center image, thatis, G_c, and the four neighboring red and green images at each side are used. The red and green images at each sampling position are defined as R_p and G_p where $\{p \mid \mathrm{n}, \mathrm{s}, \mathrm{e}, \mathrm{w}\}$, respectively, and R_p for each position is defined as follows:

$$\begin{aligned} R_{\mathrm{n}}(i, j) &= R_{10}(i-1, j), \\ R_{\mathrm{s}}(i, j) &= R_{10}(i, j), \\ R_{\mathrm{e}}(i, j) &= \mathrm{CFA}(2i, 2j+1) = R_{01}(i, j), \\ R_{\mathrm{w}}(i, j) &= \mathrm{CFA}(2i, 2j-1) = R_{01}(i, j-1). \end{aligned} \tag{22}$$

(a)

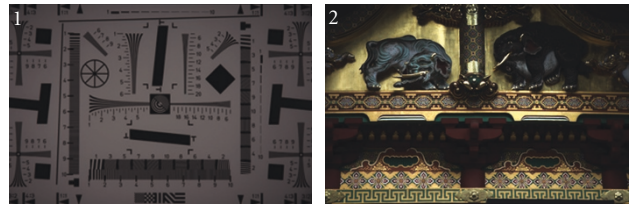

(b)

Figure 7: (a) Kodak PhotoCD image set and (b) Bayer raw data.

Considering the four neighboring red and green images of G_c, the local variation and local similarity criteria are estimated as the same way in (10) and (13) by using the newly defined $D_{G_cR_p}(i,j)$. When the edge direction is estimated by (14) and (17) with the process of region classification, R_{00} is directionally interpolated, given as:

$$R_{00} = \begin{cases} G_c - \dfrac{\omega_e K_e^R + \omega_w K_w^R}{\omega_e + \omega_w} & \text{if EDT} = \text{Hor}, \\ G_c - \dfrac{\omega_n K_n^R + \omega_s K_s^R}{\omega_n + \omega_s} & \text{if EDT} = \text{Ver}, \\ G_c - \dfrac{(\omega_n K_n^R + \omega_s K_s^R + \omega_e K_e^R + \omega_w K_w^R)}{(\omega_n + \omega_s + \omega_e + \omega_w)} & \text{if EDT} = \text{Non}, \end{cases} \tag{23}$$

where $K_p^R(i,j) = G_p(i,j) - R_p(i,j)$. The weight function is computed as the same way in (20), but the gradient values are calculated in the green LR images.

4. Experimental Results

To study performance experimentally, the proposed and other existing algorithms were tested with Kodak PhothCD image set and Bayer CFA raw data shown in Figure 7. For comparison, three groups of conventional methods were implemented: nonedge directed (nonED) methods proposed by Pei and Tam [7], by Gunturk et al. [13], and by Zhang and Wu [14], the indirect edge directed (indirect ED) methods such as primary-consistency soft-decision (PCSD) method [20], the homogeneity-directed method [21], and the a posteriori decision method [22], and the direct edge directed (direct ED) methods such as the variance of color differences method [23], and the adaptive heterogeneity-projection method [25]. They were implemented following the parameters given in each paper or using the provided source code [14]. Also, we implemented each of the methods without the refining step [21–23, 25] so that the performances of the methods were compared fairly.

The peak signal-to-noise ratio (PSNR) and the normalized color difference (NCD) were used for quantitative measurement. The PSNR is defined in decibels as $\text{PSNR} = 10\log_{10}(255^2/\text{MSE})$, where MSE represents the mean squared error between the original and the resultant images. The NCD is an objective measurement of the perceptual errors between the original and the demosaicked color images [11]. This value is computed by using the ratio of the perceptual color errors to the magnitude of the pixel vector of the original image in the CIE Lab color space. A smaller NCD value represents that a given image is interpolated with a reduced color artifact. In Tables 1 and 2, PSNR and NCD values of each algorithm were compared. Among the conventional methods, nonED methods, such as DLLMMSE [14] and POCS [2], show high performance in terms of the numerical values. Also, the recent edge directed techniques [21–23, 25] show high PSNR and NCD performance among the conventional edge directed techniques, especially in the images with fine texture patterns, such as *Kodak 5, 6, 8, 15*, and *19*. The proposed method outperforms the conventional edge directed methods in the majority of the images including those challenging images with 0.345–2.191 dB and 0.003–0.203 improvements of the averaged PSNR and NCD values, respectively.

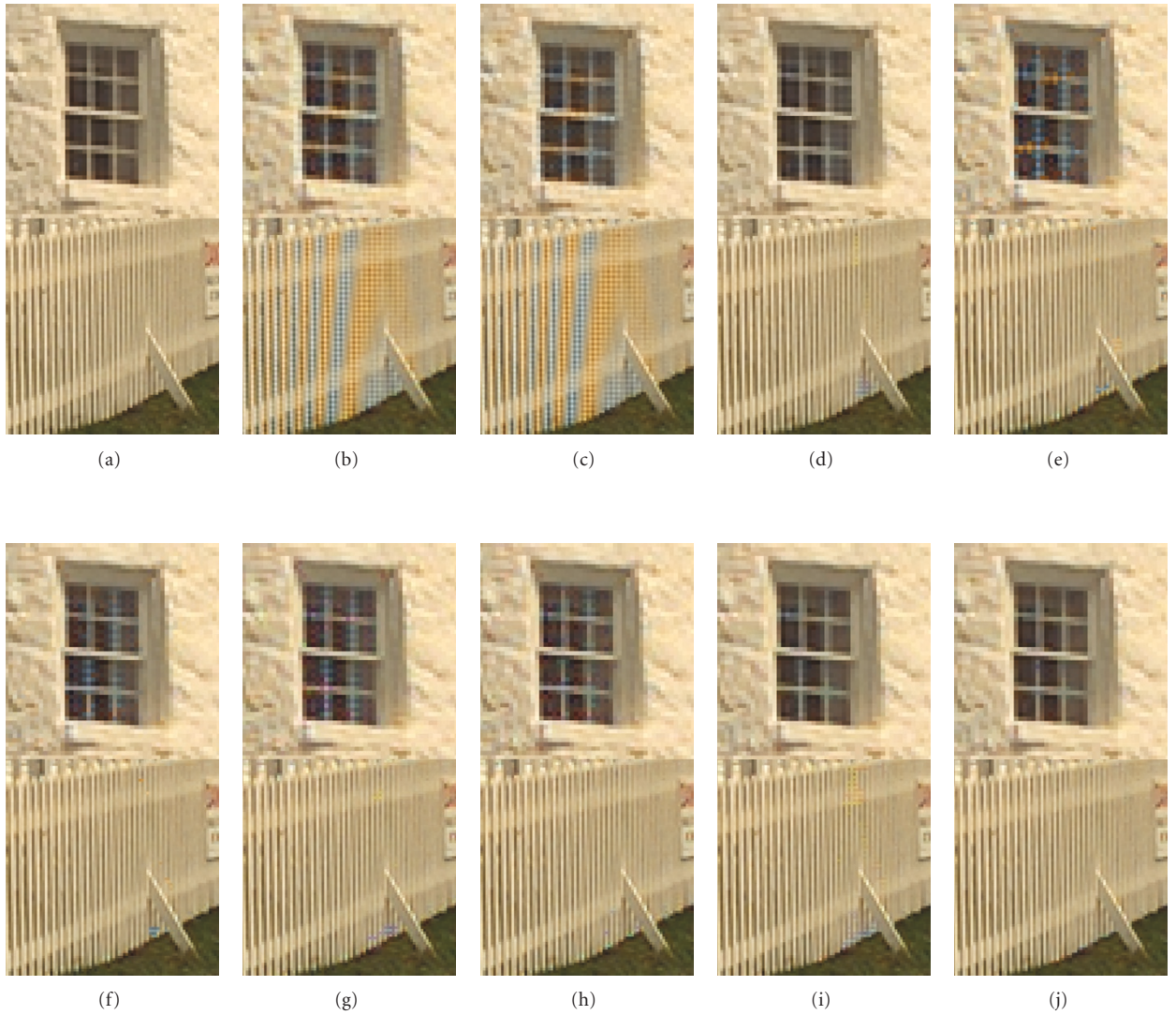

Figure 8: The partially magnified images of *Kodak 19* from (a) the original image, and from the results of (b) Pei [7], (c) the POCS [13] (d) the directional LMMSE [14], (e) the PCSD [20], (f) the homogeneity-directed [21], (g) a posteriori decision [22], (h) the variance of color differences [23], (i) the adaptive heterogeneity-projection [25], and (j) the proposed method.

To show the performance of each methods in edge patterns and edge junctions, the resulting images are shown in Figures 8–11 that contain fine textures of *Kodak 19, 15* and real images, respectively. At first, the competitive regions of *Kodak 19* are shown in Figure 8. In each of the image crop, the vertically directed line edge pattern of the fence and the edge junctions of the window are depicted. In spite of the high PSNR performance, POCS method shows the Moiré pattern and the zipper artifacts in Figure 8(c). In Zhang's method and the edge directed methods in Figures 8(d)–8(i), the fence regions are highly improved with reduced errors. However, visible artifacts were remained on the vertical edges of the high frequency region or boundaries between the fence and the grass. Moreover, the zippers and disconnection were shown in the edge junctions in the upper image crop in Figures 8(b)–8(i). In Figure 8(j), the resultant image of the proposed algorithm shows better results in terms of the clear edges and the reduced visible artifacts. The resultants of the methods in the textures with diagonal patterns or diagonal lines are shown in Figure 9. While the artifacts were produced along the ribbon boundary in Figures 9(b)–9(i), the proposed method produced consistent edges with accurate edge direction estimation.

By using the high-resolution 12-bit Bayer CFA raw data in Figure 7(b), we can demonstrate the performance of each algorithm in the presents of noise. In Figures 10 and 11, the resultant images are shown with the region which contains edge junctions. In these regions, most of the algorithms show zipper artifacts caused by the false estimation of

Table 1: The PSNR comparison of the conventional and proposed methods using the average of the three channels (dB) on the 24 test images in Figure 7(a).

	NonED			Indirect ED			Direct ED		
	[7]	[13]	[14]	[20]	[21]	[22]	[23]	[25]	Proposed
1	34.036	37.080	38.781	33.733	35.333	35.335	35.379	36.090	36.421
2	39.142	39.639	41.237	39.173	39.525	40.010	39.446	40.748	40.746
3	41.190	41.760	42.956	40.777	41.974	42.232	41.771	42.611	42.757
4	39.950	40.616	41.289	38.965	39.860	39.878	39.837	40.415	40.530
5	35.512	37.406	38.263	35.023	36.338	36.440	35.890	36.853	37.431
6	35.206	38.159	40.458	35.083	38.001	38.070	37.661	38.290	38.589
7	40.704	41.686	42.277	41.016	41.267	41.490	40.935	42.130	42.708
8	30.974	34.487	36.385	32.293	33.969	33.934	34.059	34.539	35.596
9	39.785	41.298	42.813	40.277	41.371	41.526	41.314	41.748	42.292
10	40.265	41.562	42.277	39.841	41.038	41.174	40.717	41.276	41.738
11	36.596	39.000	40.236	36.298	37.947	37.988	37.648	38.661	39.087
12	40.300	42.325	43.653	40.866	42.238	42.500	42.032	42.732	42.899
13	31.545	34.096	35.062	29.857	31.951	31.643	31.791	32.417	32.781
14	35.940	36.280	37.198	35.823	35.954	36.402	36.209	37.263	37.270
15	38.811	39.492	40.133	37.682	38.871	39.003	38.842	39.250	39.662
16	38.327	41.454	44.026	38.664	41.982	42.009	41.486	41.761	42.358
17	39.367	40.850	41.611	38.542	39.920	39.693	39.512	40.213	40.663
18	35.364	36.714	37.210	33.898	35.225	34.942	34.860	35.699	36.112
19	35.512	38.511	40.809	37.338	38.677	38.688	38.667	39.503	39.958
20	38.954	40.596	41.442	38.547	39.543	39.400	39.299	40.376	40.702
21	36.039	38.558	39.502	35.396	36.923	36.694	36.723	37.675	38.035
22	36.941	37.766	38.507	36.564	37.119	37.339	36.970	37.832	38.169
23	42.118	42.186	43.297	42.107	42.322	42.628	42.407	42.595	43.217
24	33.905	34.871	35.765	32.232	34.168	33.913	33.630	34.164	34.467
avg.	37.353	39.016	40.216	37.083	38.397	38.455	38.212	38.952	39.341

the edge direction. Among the conventional methods, edge directed techniques such as the variance of color differences method and the adaptive heterogeneity-projection method in Figures 10(g) and 10(h) demonstrates good performance on the horizontal and vertical directional edges. Similar results are shown in the diagonal edges in Figures 11(g) and 11(h). However, some artifacts are remained in the edge direction changing regions. In the resultants of the proposed method in Figures 10(i) and 11(i), the interpolated pixels are consistent along the edge and this shows the robustness of the spatial correlation of the Bayer color difference based method.

To show the computational requirements, the averaged run times of 24 images from Kodak PhotoCD image set for each algorithm are calculated in Table 3. The experiments were performed on a PC equipped with an Intel Core2 Duo E8400 CPU. In the table, the processing time is increased depending on the estimation criterion: for example, preinterpolation before estimation and a posteriori decision [22] or the adaptive range of neighborhood for gradient calculation [23] needed more time than the simple estimation [7]. The proposed method consumed more time than these methods due to the multiple steps of the edge oriented region classifier. However, it consumed less time than the homogeneity-directed method [21], minimum mean square error-based interpolation method [14], and the adaptive heterogeneity-projection method [25] while the image qualities were highly improved.

5. Conclusion

In this paper, we have proposed the edge adaptive color demosaicking algorithm that effectively estimates the edge direction on the Bayer CFA samples. We examined the spatial correlation on the Bayer color difference plane, and proposed the criteria for the region classification and the

Table 2: The NCD comparison of the conventional and proposed methods on the 24 test images in Figure 7(a).

	NonED			Indirect ED			Direct ED		
	[7]	[13]	[14]	[20]	[21]	[22]	[23]	[25]	Proposed
1	3.372	2.724	1.994	3.286	2.663	2.924	2.789	2.517	2.426
2	2.311	2.244	1.905	2.201	2.177	2.133	2.179	1.910	1.906
3	1.409	1.321	1.211	1.428	1.311	1.318	1.333	1.231	1.212
4	1.876	1.800	1.725	2.051	1.897	1.950	1.924	1.777	1.764
5	4.217	3.491	3.040	4.105	3.608	3.821	3.843	3.329	3.152
6	2.373	1.939	1.384	2.206	1.636	1.751	1.782	1.636	1.565
7	1.677	1.553	1.458	1.554	1.563	1.535	1.569	1.431	1.347
8	4.064	3.158	2.246	3.271	2.780	3.004	2.847	2.567	2.364
9	1.352	1.183	1.028	1.271	1.144	1.175	1.158	1.131	1.066
10	1.342	1.203	1.124	1.369	1.238	1.282	1.279	1.223	1.168
11	3.014	2.526	2.056	2.798	2.403	2.499	2.528	2.227	2.142
12	1.006	0.887	0.744	0.958	0.830	0.857	0.865	0.810	0.784
13	4.737	3.898	3.313	5.648	4.387	4.991	4.707	4.208	4.032
14	3.203	2.918	2.593	3.160	2.969	3.034	2.972	2.647	2.595
15	2.148	2.052	1.958	2.329	2.155	2.201	2.183	2.018	1.980
16	2.150	1.749	1.218	1.918	1.409	1.507	1.525	1.499	1.386
17	2.663	2.363	2.207	2.771	2.490	2.631	2.578	2.465	2.333
18	4.152	3.828	3.720	4.711	4.284	4.440	4.397	4.019	3.833
19	2.528	2.126	1.661	2.321	2.011	2.135	2.065	1.897	1.792
20	1.483	1.303	1.155	1.522	1.356	1.443	1.411	1.264	1.216
21	2.393	1.989	1.684	2.511	2.078	2.292	2.212	1.965	1.891
22	2.133	2.007	1.884	2.289	2.125	2.167	2.197	1.983	1.909
23	1.261	1.245	1.216	1.290	1.307	1.284	1.286	1.248	1.187
24	2.514	2.239	1.968	2.684	2.310	2.472	2.430	2.199	2.114
avg.	2.474	2.156	1.854	2.486	2.172	2.285	2.253	2.050	1.965

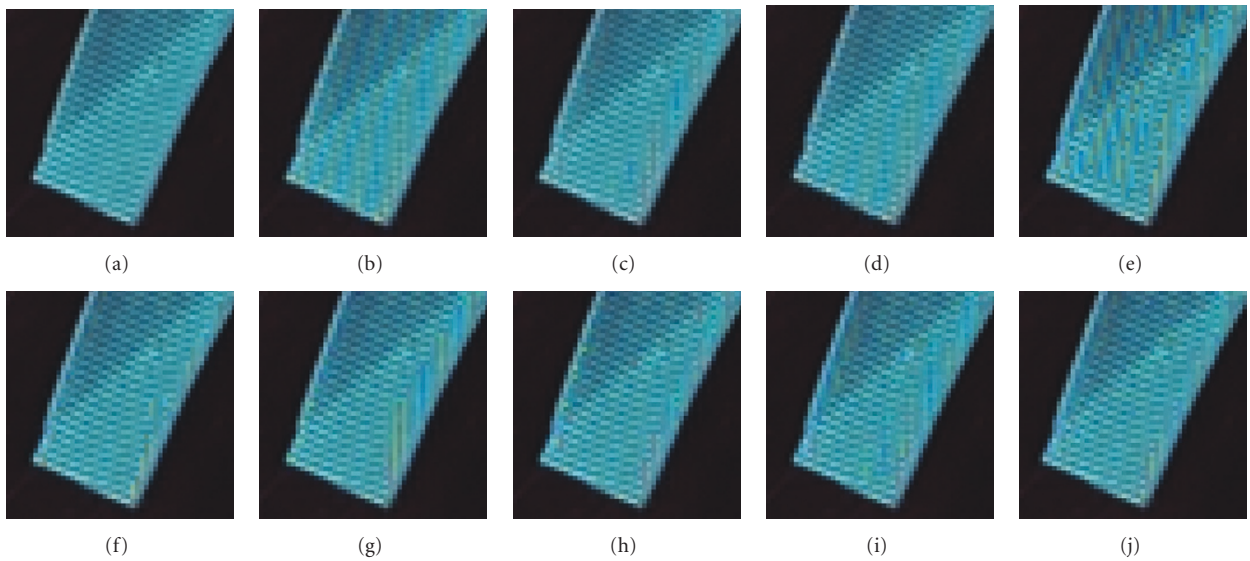

Figure 9: The partially magnified images of *Kodak 15* from (a) the original image, and from the results of (b) Pei [7], (c) the POCS [13] (d) the directional LMMSE [14] (e) the PCSD [20], (f) the homogeneity-directed [21], (g) a posteriori decision [22], (h) the variance of color differences [23], (i) the adaptive heterogeneity-projection [25], and (j) the proposed method.

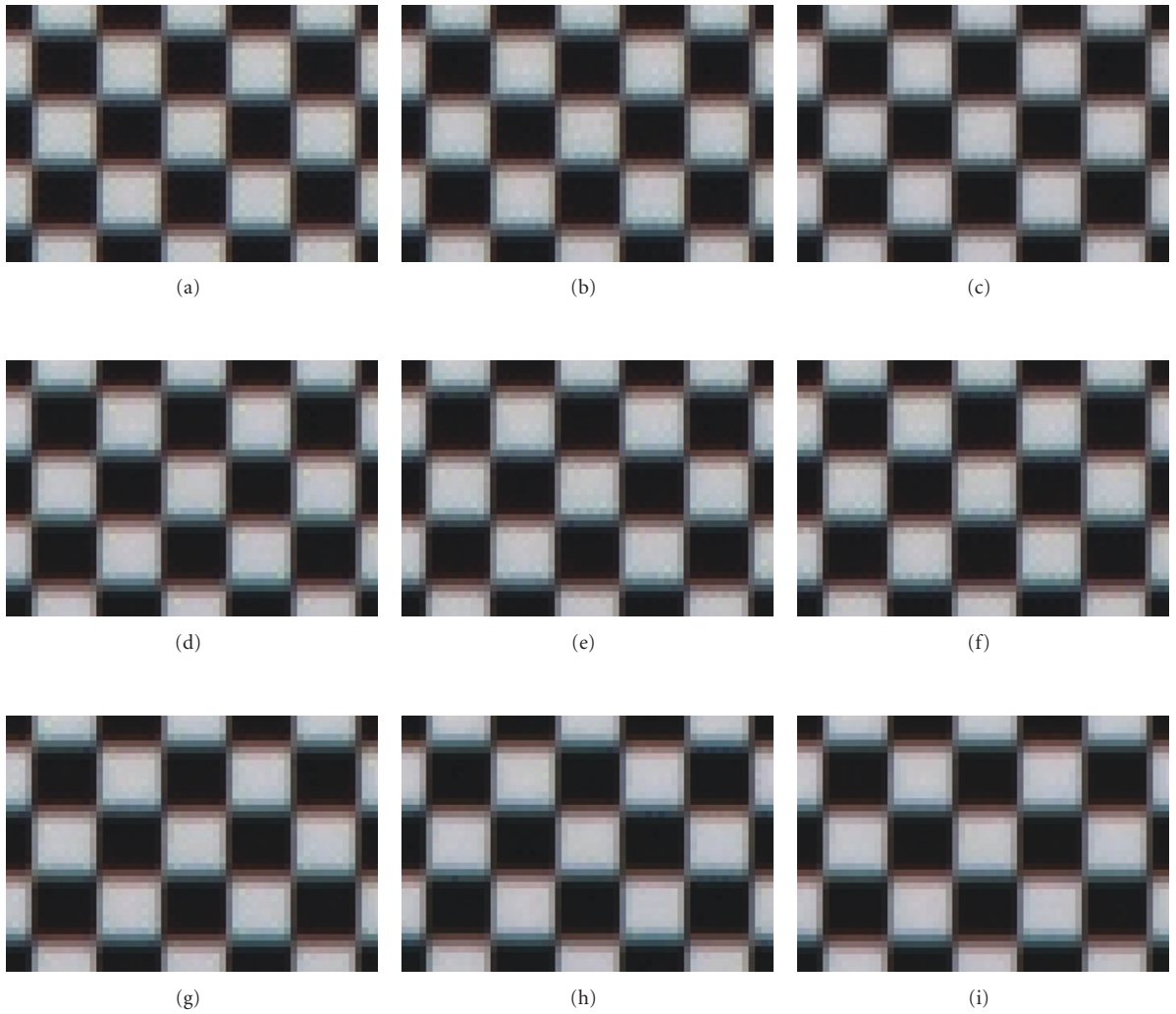

Figure 10: The results of Bayer CFA raw data 1 of (a) Pei [7], (b) the POCS [13], (c) the directional LMMSE [14], (d) the PCSD [20], (e) the homogeneity-directed [21], (f) a posteriori decision [22], (g) the variance of color differences [23], (h) the adaptive heterogeneity-projection [25], and (i) the proposed method.

Table 3: Computational complexity comparison for the presented color demosaicing methods (measured in seconds on an Intel Core2 Duo E8400 processor).

Method	[7]	[13]	[14]	[20]	[21]	[22]	[23]	[25]	Proposed
Time (s)	0.025	5.221	0.404	0.267	0.384	0.065	0.221	0.469	0.325

edge direction estimation. To estimate the edge direction in the complicated edge regions, the proposed method classified regions of an image into three types: edge, edge pattern, and flat regions. According to the edge types, the edge direction were effectively estimated and the directional interpolation resulted in clear edge. The proposed edge adaptive demosaicking method improved the overall image quality in terms of consistent edge directions around the edges. The proposed method was compared with the conventional edge directed and nonedge directed methods on the several images including the Bayer raw data. The simulation results indicated that the proposed method outperforms conventional edge directed algorithms with respect to both objective and subjective criteria.

Acknowledgments

This research was supported by Mid-career Researcher Program through the NRF(National Research Foundation

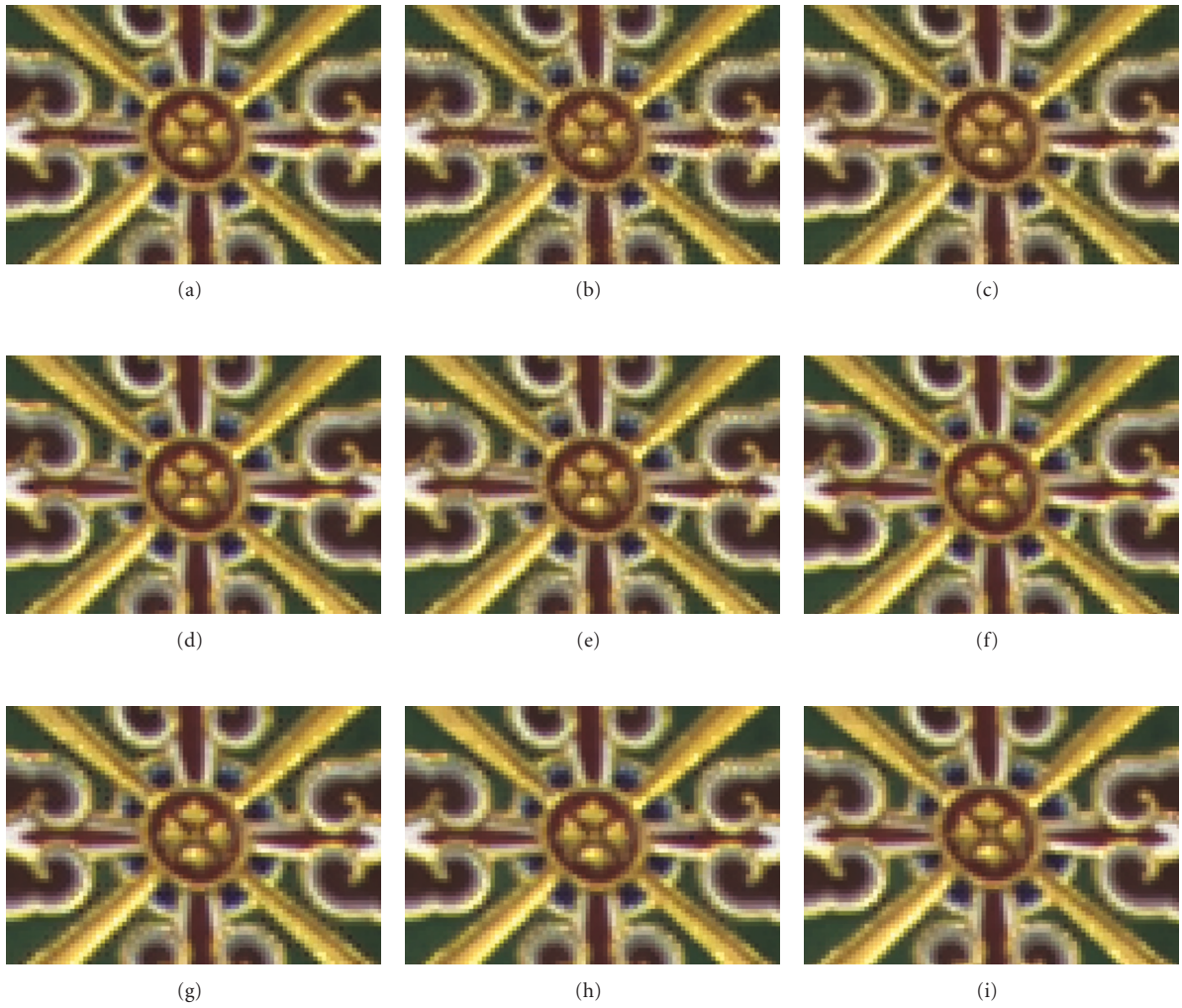

Figure 11: The results of Bayer CFA raw data 2 of (a) Pei [7], (b) the POCS [13], (c) the directional LMMSE [14], (d) the PCSD [20], (e) the homogeneity-directed [21], (f) a posteriori decision [22], (g) the variance of color differences [23], (h) the adaptive heterogeneity-projection [25], and (i) the proposed method.

of Korea) grant funded by the MEST (no. 2010-0000345) and by the MKE(The Ministry of Knowledge Economy), Korea, under the ITRC (Information Technology Research Center) support program supervised by the NIPA(National IT Industry Promotion Agency) (NIPA-2010-(C1090-1011-0003)).

References

[1] B. E. Bayer, "Color imaging array," US patent no. 3 971 065, July 1976.

[2] B. K. Gunturk, J. Glotzbach, Y. Altunbasak, R. W. Schafer, and R. M. Mersereau, "Demosaicking: color filter array interpolation," *IEEE Signal Processing Magazine*, vol. 22, no. 1, pp. 44–54, 2005.

[3] D. R. Cok, "Signal processing method and apparatus for producing interpolated chrominance values in a sampled color image signal," US patent no. 4 642 678, February 1987.

[4] R. Lukac, K. Martin, and K. N. Plataniotis, "Demosaicked image postprocessing using local color ratios," *IEEE Transactions on Circuits and Systems for Video Technology*, vol. 14, no. 6, pp. 914–920, 2004.

[5] J. E. Adams Jr., "Interactions between color plane interpolation and other image processing functions in electronic photography," in *Cameras and Systems for Electronic Photography and Scientific Imaging*, vol. 2416 of *Proceedings of SPIE*, pp. 144–151, February 1995.

[6] J. E. Adams Jr., "Design of practical color filter array interpolation algorithms for digital cameras, Part 2," in *Proceedings of the International Conference on Image Processing (ICIP '98)*, pp. 488–492, October 1998.

[7] S.-C. Pei and I.-K. Tam, "Effective color interpolation in CCD color filter arrays using signal correlation," *IEEE Transactions on Circuits and Systems for Video Technology*, vol. 13, no. 6, pp. 503–513, 2003.

[8] R. Kimmel, "Demosaicing: image reconstruction from color CCD samples," *IEEE Transactions on Image Processing*, vol. 8, no. 9, pp. 1221–1228, 1999.

[9] B. S. Hur and M. G. Kang, "Edge-adaptive color interpolation algorithm for progressive scan charge-coupled device image sensors," *Optical Engineering*, vol. 40, no. 12, pp. 2698–2708, 2001.

[10] W. Lu and Y.-P. Tan, "Color filter array demosaicing: new method and performance measures," *IEEE Transactions on Image Processing*, vol. 12, no. 10, pp. 1194–1210, 2003.

[11] S. W. Park and M. G. Kang, "Color interpolation with variable color ratio considering cross-channel correlation," *Optical Engineering*, vol. 43, no. 1, pp. 34–43, 2004.

[12] C. W. Kim and M. G. Kang, "Noise insensitive high resolution color interpolation scheme considering cross-channel correlation," *Optical Engineering*, vol. 44, no. 12, Article ID 127006, 2005.

[13] B. K. Gunturk, Y. Altunbasak, and R. M. Mersereau, "Color plane interpolation using alternating projections," *IEEE Transactions on Image Processing*, vol. 11, no. 9, pp. 997–1013, 2002.

[14] L. Zhang and X. Wu, "Color demosaicking via directional linear minimum mean square-error estimation," *IEEE Transactions on Image Processing*, vol. 14, no. 12, pp. 2167–2178, 2005.

[15] D. Alleysson, S. Süsstrunk, and J. Hérault, "Linear demosaicing inspired by the human visual system," *IEEE Transactions on Image Processing*, vol. 14, no. 4, pp. 439–449, 2005.

[16] C. A. Laroche and M. A. Prescott, "Apparatus and method for adaptively interpolating a full color image utilizing chrominance gradients," US patent no. 5 373 322, December 1994.

[17] R. H. Hibbard, "Apparatus and method for adaptively interpolating a full color image utilizing luminance gradients," US patent no. 5 382 976, January 1995.

[18] J. E. Adams and J. F. Hamilton Jr., "Adaptive color plane interpolation in single color electronic camera," US patent no. 5 506 619, April 1996.

[19] J. E. Adams Jr., "Design of practical color filter array interpolation algorithms for digital cameras," in *Real-Time Imaging II*, vol. 3028 of *Proceedings of SPIE*, pp. 117–125, February 1997.

[20] X. Wu and N. Zhang, "Primary-consistent soft-decision color demosaicking for digital cameras (patent pending)," *IEEE Transactions on Image Processing*, vol. 13, no. 9, pp. 1263–1274, 2004.

[21] K. Hirakawa and T. W. Parks, "Adaptive homogeneity-directed demosaicing algorithm," *IEEE Transactions on Image Processing*, vol. 14, no. 3, pp. 360–369, 2005.

[22] D. Menon, S. Andriani, and G. Calvagno, "Demosaicing with directional filtering and a posteriori decision," *IEEE Transactions on Image Processing*, vol. 16, no. 1, pp. 132–141, 2007.

[23] K.-H. Chung and Y.-H. Chan, "Color demosaicing using variance of color differences," *IEEE Transactions on Image Processing*, vol. 15, no. 10, pp. 2944–2955, 2006.

[24] C.-Y. Tsai and K.-T. Song, "Heterogeneity-projection hard-decision color interpolation using spectral-spatial correlation," *IEEE Transactions on Image Processing*, vol. 16, no. 1, pp. 78–91, 2007.

[25] K.-L. Chung, W.-J. Yang, W.-M. Yan, and C.-C. Wang, "Demosaicing of color filter array captured images using gradient edge detection masks and adaptive heterogeneity-projection," *IEEE Transactions on Image Processing*, vol. 17, no. 12, pp. 2356–2367, 2008.

[26] L. Zhang, R. Lukac, X. Wu, and D. Zhang, "PCA-based spatially adaptive denoising of CFA images for single-sensor digital cameras," *IEEE Transactions on Image Processing*, vol. 18, no. 4, pp. 797–812, 2009.

[27] L. Zhang, X. Wu, and D. Zhang, "Color reproduction from noisy CFA data of single sensor digital cameras," *IEEE Transactions on Image Processing*, vol. 16, no. 9, pp. 2184–2197, 2007.